***ARCHER***

*Collaborative Project (CP)*

Co-funded by the European Commission under the Euratom Research and Training Programme on Nuclear Energy within the Seventh Framework Programme

Grant Agreement Number : 269892

Start date : 01/02/2011 Duration : 48 Months
www.archer-project.eu

# Report on the variations in pebble bed stacking in HTRs

Authors : Gert Jan Auwerda and
KLOOSTERMAN Jan-Leen (TUDelft)

ARCHER - Contract Number: 269892
Advanced High-Temperature Reactors for Cogeneration of Heat and Electricity R&D
EC Scientific Officer: Dr. Panagiotis Manolatos

| | |
|---|---|
| Document title | Report on the variations in pebble bed stacking in HTRs |
| Author(s) | Gert Jan Auwerda, KLOOSTERMAN Jan-Leen |
| Number of pages | 25 |
| Document type | Deliverable |
| Work Package | WP 24 |
| Document number | D24.41 |
| Issued by | TU Delft |
| Date of completion | 07/10/2013 |
| Dissemination level | Restricted to a group specified by the consortium (including the Commission Services). |

**Summary**

In pebble bed type nuclear reactors the fuel pebbles form a randomly stacked bed with a non-uniform packing density. To investigate flow and heat transfer through these beds and develop realistic models, we need a good understanding of the nature of randomly stacked beds and validated computational methods that can generate realistic beds. To this end we accurately measured the average packing fraction and radial and axial packing fraction profiles of a bed containing 5400 acrylic pebbles with a diameter of 12.7 mm. In a second experiment we determined the pebble locations of a bed containing 8900 glass pebbles with diameters of 1.66-2.00 mm using 3D X-ray tomography, from which various microscopic stacking properties were evaluated for both the bulk of the bed away from the wall and in the near wall region. Results were used to validate a computed bed, generated using a method based on the removal of overlaps.
Results for the computed bed are in good agreement with the experiments and with literature, giving confidence that the method is capable of generating beds with realistic packing structures, although the experimental results for the microscopic stacking properties in the near wall region are of insufficient quality for a meaningful comparison. Analysis of the various results shows different stacking properties near the wall than in the bulk of the bed, indicating the stacking is anisotropic near a boundary forming semi-ordered layers parallel to the wall with hexagonal-like stacking properties, which implies flow and heat transfer might be anisotropic near the wall and could need different models near the wall than in the bulk to be accurately described. Finally, the probability distribution of packing fractions of small clusters of around 45 pebbles showed that the local packing fraction inside a packed bed can vary strongly, both in the bulk and near the wall, which might significantly affect flow rates and could result in hotspots.

Approval

| Date | By |
|---|---|
| 08/10/2013 | Michael BUCK |
| 10/10/2013 | Norbert KOHTZ |
| 15/10/2013 | Sander DE GROOT |

Distribution list

| Name | Organisation | Comments |
|---|---|---|
| P. Manolatos | EC DG RTD | Through the EC participant portal |
| All beneficiaries | ARCHER | Through the private online workspace |

**Table of contents**

# 1 Introduction

In pebble bed calculations the bed is commonly modelled as a fully homogenised mixture of coolant and pebble materials using a uniform packing fraction. However, it is well known that the packing density of randomly stacked beds is not uniform, but exhibits strong fluctuations near solid boundaries, see for example [1]. The effect of the non-uniform pebble distribution can be significant for both neutronics, due to neutron streaming for example [2,3], as well as thermodynamics, for example due to the wall channelling effect of the coolant flow [4].

Over the years, several experiments have been performed to measure void fractions in packed beds, see for example [1]. Lately, computational methods to generate randomly stacked pebble beds got more attention. Du Toit [5] applied a Discrete Elements Method (DEM) to generate void fraction profiles in pebble beds for thermohydraulics studies, and both Cogliati [6] and Rycroft [7] used DEM to simulate pebble flow in pebble bed reactors. Kloosterman [8] applied a Monte Carlo rejection method to generate pebble bed stackings for the calculation of spatially-dependent Dancoff factors, and we [3] used a method of removing overlaps to generate beds to investigate neutron streaming in the PROTEUS experimental facility.

However, these studies only looked at radial and axial profiles, while a good understanding of the pebble-to-pebble microstructure of randomly packed beds is also important for various subjects. For example, the coordination number, the number of pebbles touching a certain pebble, was used by Van Antwerpen et al. [9] to develop a model to calculate the effective thermal conductivity of a packed bed. Also, detailed CFD analysis of small sections of the bed, with pebbles modelled explicitly such as in [10], can be an aid in developing better models and gaining a better understanding of flow and heat transfer effects in pebble beds, but require a realistic configuration of the pebbles. Finally, due to the stochastic nature of the pebble bed, local variations in packing fraction will occur, see for example [11]. These variations are a possible cause of hotspots, as a local densification in the packing will result in both a bigger resistance to coolant flow and a higher power density. If we want to analyse these non-uniformity's and their effects on fuel temperature, a good description of local variations of the packing fraction is needed. To better investigate the above mentioned subjects, it is desirable to be able to computationally generate packed beds of arbitrary shapes and sizes which accurately capture both the macroscopic properties such as average packing fraction and radial packing fraction distribution, as well as the local microstructure in a randomly stacked bed.

When looking at computer generated beds, various authors have described not only global properties, but also local properties of the stacking microstructure [12,13]. However, validation of the results by comparison with experimental data was not always given. Only recently, accurate experimental data of the microscopic packing structure of randomly stacked beds has become available through the use of computer aided X-ray tomography, where especially the work of Aste [14] stands out because of the large size of the samples (up to 143,000 pebbles). Unfortunately, Aste only looked at the packing structure in the bulk of the bed far away from the walls, while in pebble bed reactors we are also interested in the packing microstructure near the wall.

The goal of this study is twofold. First, validate the packing structure of our computer generated beds both on a macroscopic and on a pebble-to-pebble level, by comparing the radial and axial packing fraction profiles and average packing fraction with measured profiles, and by comparing various microscopic stacking properties in both the bulk of the bed and near the wall with literature and with experimental results. The second goal is to investigate the local variations in packing fraction in randomly packed beds, by calculating the probability density function of the packing fraction of small clusters of pebbles in both the bulk of the bed and near the wall, for both a computed bed and experimental results.

For validation purposes two sets of experiments were performed. The first used a non-destructive method to measure very accurately the radial and axial void fraction profiles of a randomly stacked pebble bed with the PebBEx facility, see Section 2, which results are compared in Section 4 with the profiles of a computer generated bed created with a method of removing overlaps described in Section 3. Additionally a pebble-by-pebble image of a pebble bed containing almost 9000 pebbles was created using X-ray tomography, as detailed in Section 5. Stacking properties of the bed were investigated for both the inner zone away from the wall and the outer zone close to the wall, and compared with those of a computer generated bed. The packing microstructure of the beds is evaluated in Section 6 by looking at the probability distributions of various properties of the local packing. First we look at the coordination number, the average number of spheres in contact with a given sphere, followed by the distribution of Voronoï polyhedra, the radial distribution function, and finally the distribution of angles between the contact lines of pebbles with their common neighbour. Next, we investigate in Section 7 the variation in local packing fraction in the pebble beds. Here the local packing fraction is the average packing fraction of a small area of four to five pebbles in diameter. Distributions of the local packing fractions were calculated and compared for the inner and outer zone of both the generated and scanned beds. Finally Section 8 contains the conclusions on how realistic the computer generated bed is and on the observed variations in local packing fractions.

# 2 The PebBEx Facility

The Pebble Bed Experimental facility (PebBEx) at the Reactor Institute Delft (RID) of the Delft University of Technology has been developed to measure void fraction profiles of packed beds of pebbles using gamma-ray scanning [15]. See Figure 1 for a schematic overview and photograph of the setup. The setup consists of a cylindrical vessel of acrylic plastic, with a height of 235 mm and an inner diameter of $D$=229 mm. The vessel can be filled with acrylic pebbles of various sizes. For this experiment pebbles of $d$=12.7 mm were used, resulting in a $D/d$ ratio of 18.0. The void fraction of the pebble bed is measured using the main gamma peak at 59.5 keV of an Am-241 source. The attenuation coefficient of the used acrylic (PMMA) for this energy was experimentally determined to be 0.229 ± 0.004 $cm^{-1}$ [16].

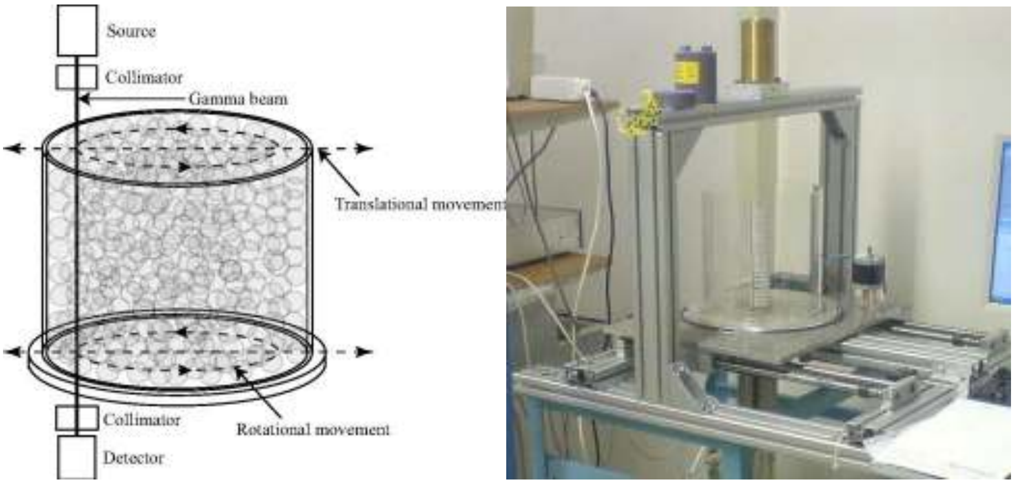


Figure 1: Schematic overview and photograph of the PebBEx facility, for measuring the radial void fraction profile.

During the radial void fraction measurements the source is located above the experiment, followed by a collimator with a diameter of 1 mm, creating a narrow beam downwards through the pebble bed. Below the pebble bed the intensity of the beam is measured using a NaI(TI) scintillation detector, topped by a second collimator. From the measured intensity of the beam the amount of acrylic in the path of the gamma beam can be calculated. The vessel itself can be rotated and moved sideways using two electrical stepmotors. By measuring the void fraction while rotating the vessel the (average) radial void fraction at a certain distance from the wall can be measured. Moving the vessel sideways in between the radial void fraction measurements allows measuring the void fraction at various radial positions.

Later, the PebBEx facility was adjusted to allow the measurement of the axial void fraction of a pebble bed. To this end, the source and detector were attached to the sides of the bridge in Figure 1, with the possibility to move them up and down using a step motor and threaded rod, similar to the mode of shifting the pebble bed in the horizontal direction, see Figure 2. At each vertical position from the bottom of the bed, the void fraction was measured at >250 horizontal locations by moving the bed with steps of 1 mm in horizontal direction. The value of the void fraction at the vertical position was then calculated by a weighted sum of these measurements, using the distance the beam travelled through the pebble bed ($l_x$ in Figure 2) at each horizontal position as a weight factor, and compensating for the changing distance the beam travelled through the cylindrical wall of the vessel.

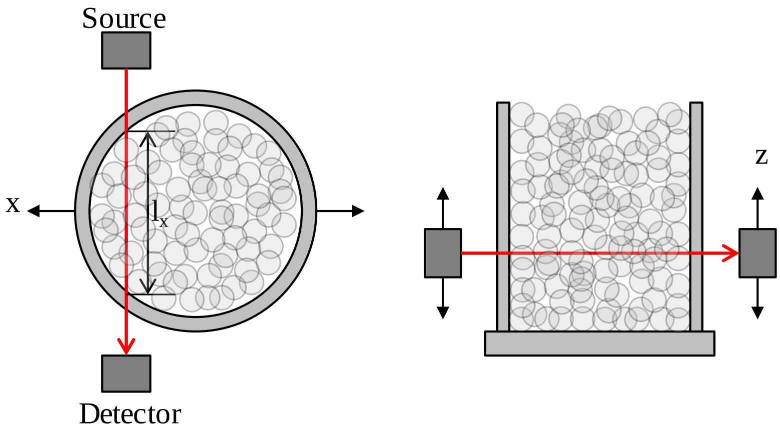

Figure 2: Schematic overview of PebBEx for measuring the axial void fraction profile (collimators not shown).

# 3 Computational Method

In literature various numerical methods are described to generate randomly packed pebble beds. These include rigorous algorithms that simulate pebble flow as accurately as possible based on physics laws, for example the Discrete Elements Method (DEM) [6], and synthetic techniques, such as the Monte Carlo rejection method [8] and the overlap removal method [12]. Each of these methods has its own advantages and disadvantages. In our research we have developed a method based on the overlap removal method as described by Mrafko [1]2, as in this method overlaps of pebbles are easily avoided, it is relatively fast for the generation of small to medium sized beds, and is straightforward to implement.

The method consists of removing overlaps between the spheres by moving them apart, starting from a randomly generated overly dense packing of overlapping spheres. After removing all overlaps, the pebble radius is increased to its desired radius in $N$ steps, while in each step the algorithm eliminates new overlaps among the spheres.

In the initialization step the pebble coordinates of the $N_{peb}$ pebbles are generated inside the cylinder containing the pebble bed. This is done by generating $N_{peb}$ random points in a volume at the bottom of the cylinder, disregarding possible overlaps. To make sure the initial distribution of pebbles is dense, the volume in which the pebbles are generated is equal to that of the $N_{peb}$ pebbles at their initial radius $R_{ini}$.

The pebble radius is increased in $N$ steps from its initial value $R_{ini}$ to the desired final pebble radius $R_{peb}$. The initial radius $R_{ini}$ is typically chosen to be 2/3 of $R_{peb}$. The pebble radius is increased in ever smaller steps to increase the sensitivity of the method in each step, following a logarithmic interpolation between initial and final radius

$$R_i = R_{ini} + (R_{peb} - R_{ini}) \log(1+9(i-1)/(N-1))$$

with $R_i$ the pebble radius in step $i$.

In each step overlaps between pebbles are removed by moving the pebbles apart. A loop is run over all pebbles, and for each pebble it is checked if it overlaps with a wall or the closest neighbouring pebble. If the pebble intersects with a wall it is moved perpendicular to the wall until it touches the wall. If the pebble intersects with its nearest neighbour, both pebbles are moved an equal distance apart along their line of intersection, until they are touching. When moving the pebbles it is allowed to create new overlaps. The program keeps checking all pebbles for overlaps until all overlaps are removed. When there are no more overlaps, the loop is exited and the pebble radius can be increased again, starting the next iteration.

As there is no gravity in the removing overlaps model, the interaction of the pebbles near the top of the cylinder on those below have to take on this role. To make sure the upper part of the pebble bed is still well packed and does not contain any 'floating' pebbles balancing on only one or two other pebbles, a significant amount of extra pebbles have to be simulated to interact downward. In the removing overlaps model 8500 pebbles were simulated for $N$=5 number of steps. After the calculations were finished all pebbles not completely below 235 mm were removed.

Figure 3: Computer generated pebble bed stacking inside the PebBEx facility.

# 4 Comparison of Computed Bed with PebBEx Measurements

This section contains the results of the experimental packing fraction measurements with the PebBEx facility compared with results from a computer generated bed using the method of removing overlaps described above. All results are for a 235 mm high pebble bed in a cylinder of 229 mm diameter, with a pebble diameter of 12.7 mm.

## 4.1 Average Packing Fraction $\varepsilon_0$

To fill the vessel, pebbles were quickly poured in until it was filled almost to the top, after which the last pebbles were carefully placed at the top. To make sure the pebble bed height was as uniform as possible a plate was slowly pushed over the top of the pebble bed. The surplus of spheres which could not find a place were removed from the pebble bed. Care was taken to keep the pressure at a minimum to maintain a pebble bed stacking with a free upper surface. Filling the cylinder in this way required 5457 ±10 pebbles [16]. The same bed was used for the radial packing fraction profile measurement in Section 4.2.

The number of pebbles inside the pebble bed for both the experiment and the computed bed are shown in Table 1 together with the resulting average packing fraction $\varepsilon_0$ and the inner packing fraction $\varepsilon_\infty$ of the computed bed, representing the packing fraction of an infinite packing without wall effects. This inner packing fraction was determined by calculating the average packing fraction in a cylinder with diameter 4/9 $D$ and height between 0.3$H$ and 0.8$H$ of the height of the larger cylinder containing the bed. These values were chosen such that the borders of the volume were at least five pebble diameters away from the wall and bottom of the bed, far enough to no longer contain any influence from the wall on the packing.

Table 1: Measured and calculated average packing fractions $\varepsilon_0$ and inner packing fraction.

| Method of Generation | Number of Pebbles | Average Packing Fraction $\varepsilon_0$ | Inner Packing Fraction $\varepsilon_\infty$ |
|---|---|---|---|
| Experiment | 5457 | 0.6047 | - |
| Computed bed | 5440 | 0.6028 | 0.6315 |

The average packing fraction of the computed bed $\varepsilon_0$=0.6028 was in excellent agreement with the experimental packing fraction of the PebBEx setup of $\varepsilon_0$=0.6047 ±0.0011. Both are also in good agreement with other experimental results. Benenati and Brosilow [1] found for a bed with $D/d$=14.1 an average packing fraction of $\varepsilon_0$=0.605, and for the HTR-10 pebble bed reactor with a $D/d$ ratio of 30 an average packing fraction of $\varepsilon_0$=0.609 is reported[17]. The inner packing fraction is a representation of the packing fraction for an infinite randomly stacked pebble bed without boundary effects. Scott and Kilgour [18] found for the packing fraction of an infinite randomly stacked pebble bed a value of $\varepsilon_\infty$=0.6366 by extrapolating experimental results for beds of increasing size. Comparing this value with the value in Table 1 for the inner packing fraction of the computed bed, we again see excellent agreement.

## 4.2 Radial Packing Fraction $\varepsilon_r$

The radial packing fraction $\varepsilon_r(r)$ of the PebBEx setup was measured at radial positions 0.5 mm apart. At each position the count rate was measured for two to four full rotations of the vessel. The number of rotations depended on the count rate at the detector, with count rates ranging from 3.1 counts per second half a pebble diameter from the wall to 8 cps near the wall. At low count rates, measurement times were longer to keep the uncertainty low, resulting in more rotations of the vessel. Measurements were corrected for background, with a background of 2.51 ±0.02 cps. As calibration measurements for the empty and full cylinder, measurements outside the cylinder for a packing fraction of $\varepsilon_r$=0 and through the wall of the vessel for a packing fraction of $\varepsilon_r$=1 were used. The final uncertainty in the measurements of the packing fraction at each point was between 0.5% and 5%, depending on the local count rate, with higher uncertainty at positions with a higher packing fraction. The uncertainty in the radial position is negligible due to the high precision of the step motor used to move the cylinder. The radial packing fractions of the computer generated bed was calculated from the pebble coordinates and is, together with the experimental results, shown in Figure 4.

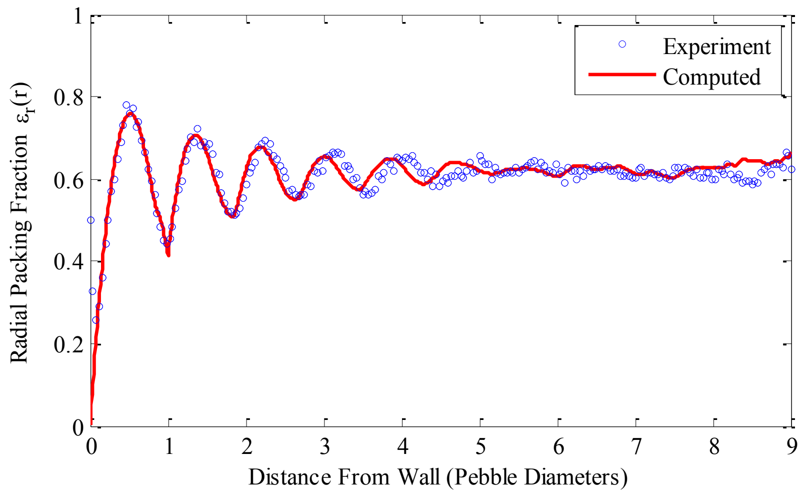


Figure 4: Radial packing fraction profile $\varepsilon_r(r)$ measured with PebBEx and for the computer generated bed.

From previous experiments we know the radial packing fraction profile is zero at the wall and reaches a maximum half a pebble diameter away from the wall [1]. The profile keeps showing these oscillations in PF further away from the wall, damping out at about 5 pebble diameters from the wall. Cause of these oscillations is the solid wall, imposing a local ordering on the pebbles, with a preferred position touching the wall. At the wall the radial packing fraction has to be zero, and due to the preferred position touching the wall, many pebbles will have their centre half a pebble diameter away from the wall, resulting in a maximum in the radial packing fraction at this location. The many pebbles touching the wall will also result in the next layer of pebbles having a high probability to be a certain distance away from this first layer, resulting in the next peak in packing fraction slightly before $r$=1.5 $d_{peb}$. These oscillations in radial PF dampen out further away from the wall, as the ordering of layers parallel to the wall becomes less and less, with no preferred ordering observable >5 $d_{peb}$ away from the wall.

Although the uncertainty per point is significant for the experimental $\varepsilon_r(r)$ measured with PebBEx, the oscillating behaviour is very clear in Figure 4 due to the large number of measuring points. The oscillations are large near the wall, with a maximum packing fraction of 0.78 half a pebble diameter from the wall. The oscillations dampen out further away from the wall and disappear at about 5 pebble diameters from the wall, just as observed in previous experiments. At the wall one would expect the packing fraction to go to zero, instead a slight increase is observed in the measurements less than 0.5 mm away from the wall. This is caused by the finite width of the gamma ray used to measure the packing fraction, created by the 1 mm wide collimator. Near the wall, part of the beam will go through the wall itself, causing additional attenuation and a higher measured packing fraction. At the other end of the measured range, at the centre of the bed, a rise in the experimental packing fraction can be observed. This is caused by the stochastic nature of the experiment itself. Near the centre of the pebble bed, the rotational path length over which the packing fraction is measured becomes very small, and thus $\varepsilon_r$ is measured over a small surface. The measurements approach that of a local point, causing larger fluctuations due to local variations in packing fraction in the pebble bed. Averaging the packing fraction near the centre over multiple experiments using different realisations of the pebble bed would result in a smooth behaviour of $\varepsilon_r$.

The radial PF profile of the computer generated bed is very similar to the measured profile. The oscillations dampen out just as fast as those in the experiment. However, the distance between the peaks of the oscillations is slightly shorter than that of the experiment. Although for the first two oscillations, up to two pebble diameters from the wall, the difference is hardly observable, after about five pebble diameters the shift in the radial position of the peaks is significant. The absence of gravity in the removing overlaps method could be the cause of this effect. As the pebbles form a close packing, they are pressed together and against the walls with no bias to direction. In reality, pebbles also experience a downward force by gravity. Since the wall is solid, pebbles can only move down by moving away from the wall, 'rolling' over the pebble below, thus slightly increasing the distance between the peaks in $\varepsilon_r$ in the radial direction.

## 4.3 Axial Packing Fraction $\varepsilon_z$

As mentioned in Section 2, after measuring the radial packing fraction profile $\varepsilon_z(r)$, the PebBEx facility was modified to measure the axial packing fraction profile $\varepsilon_z(z)$ of packed beds. For this measurement the pebble bed was filled in a different way than for the radial packing fraction measurement. Instead of quickly pouring the pebbles in the cylinder, the cylinder was slowly filled by first taking a handful of pebbles (approximately 20 each time) and carefully putting them at the bottom of the bed, repeating this process several times. After covering the bottom of the bed, the rest of the bed was filled by slowly and carefully pouring pebbles along the wall of the slightly tilted cylindrical container into the bed. As the axial packing fraction near the top of the bed was not measured, the bed was not completely filled to the top, and no measures were taken to get a flat top of the pebble bed. Unfortunately, this filling procedure meant the average packing fraction of the bed could not be calculated from the number of pebbles in the bed. To get a lower uncertainty per measurement point, a 2 mm wide collimator was used instead of the 1 mm wide collimator for the radial packing fraction measurements, resulting in a higher count rate and a much lower uncertainty in the measured packing fraction, less than 1% for all points. Measurements were performed at axial positions 1 mm apart. After measuring the axial PF profile (Measurement 1 in Figure 5), the cylinder was emptied and filled anew, and a second axial PF profile was measured (Measurement 2). To save time, the second measurement was performed faster, resulting in a higher uncertainty per measurement point of approximately 2%. For a more detailed description of the measurements see [19]. The axial packing fraction profile was also calculated for the computed bed, using the same bed as for the radial packing fraction in the previous section. The resulting measured and computed axial packing fraction profiles are given in Figure 5. To save time, $\varepsilon_z$ was measured up to a distance of $z$=8.5 $d_{peb}$ from the bottom of the bed, as the axial packing fraction more than 5 pebble diameters away from the bottom of the bed shows only statistical variations due to the stochastic nature of the bed.

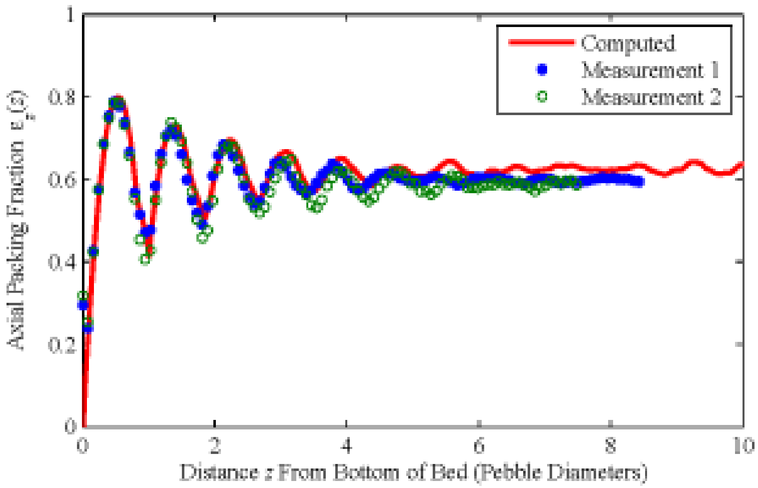


Figure 5: Axial packing fraction profile $\varepsilon_z(z)$ measured with PebBEx and for the computer generated bed.

For both measurements, the axial packing fraction in the bulk of the bed, >5 $d_{peb}$ above the bottom of the bed, is significantly lower than that of the computed bed, and also lower than the measured radial packing fraction away from the wall in Figure 5. As there was a good match between the computed bed and the radially measured packing fraction, we conclude that the average packing fraction of the beds for the axial measurement was lower than that of the bed used for the radial measurement. This lower average PF is most likely caused by the more gentle method in filling the beds for the axial measurements, resulting in less movement of the pebbles during filling.

As expected, the axial PF profiles close to the bottom of the bed are very similar to the radial PF profile, with similar minima and maxima, again damping out after about 5 pebble diameters away from the bottom. The match of the measurements with the computed bed is very good, especially for the second measurement. More than two pebbled diameters from the bottom, the peaks of the first measurement are slightly closer together and as a result lie at a lower axial position. As mentioned in the previous section, this could be due to gravity, as this will force pebbles more strongly downward, causing the partly ordered layers parallel to the wall to lie closer together than for the radial PF profile. However, the second measurement shows minima and maxima locations matching those of the computed bed, indicating that the stochastic nature of packed beds can result in significant variations in the packing fraction profiles, especially for a relatively small bed as in this experiment. For larger beds one would expect less variations between packing fraction profiles of different beds, although it should be noticed that locally variations will still exist.

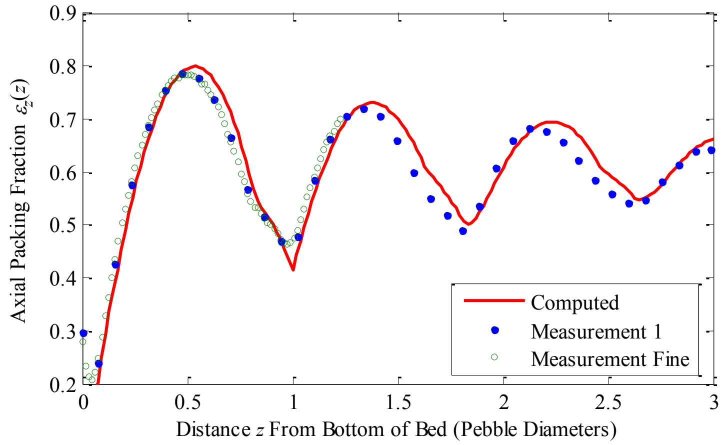


Figure 6: Course and fine measurement of the Axial packing fraction profile $\varepsilon_z(z)$ measured with PebBEx compared with that of the computer generated bed.

To get a more accurate description of the shape of the axial packing fraction profile near the wall, the PF of the first bed was measured in steps of 0.2 mm in the $z$-direction. Results are in Figure 6, together with the original, courser measurement and the computed profile. The first thing to notice is the exact match between measurement 1 and the fine measurement, proof of the reproducibility and accuracy of the measurement method. There is also a very good match with the shape of the PF profile of the computed bed. Although the minimum at $z$=1 $d_{peb}$ does not show the same sharp peak for the measurement as for the computed bed, it would be hard to reproduce with the measurement method, due to the width of the collimator. In literature the PF profile near a wall has sometimes been described using a sine or other periodic functions [20], however, we can see from Figure 5 that this is not correct. First, the profile decreasing to a minimum is not smooth, but starts to decrease more slowly close to a minimum. Second, the distance from a maximum to a minimum is around 0.5 $d_{peb}$, but the distance from a minimum to a maximum in positive $z$-direction is smaller, around 0.35 $d_{peb}$. The reason is the semi-ordered sheets of pebbles parallel to the bottom of the bed. The first maximum in PF at $z$=0.5 $d_{peb}$ is at the location of many pebble centres touching the bottom. The first minimum is at $z$=1 $d_{peb}$, 0.5 $d_{peb}$ from the location of the pebble centres of the first layer. Above this layer, a next layer of pebbles has a preferred position, slightly embedded in between the first layer. This layer has a preferred pebble centre at the location of the second maximum, which is less than 0.5 $d_{peb}$ from the minimum at $z$=1 $d_{peb}$, as the pebbles of this second layer lie in between the pebbles of the first. This is also the reason of the change in shape of the profile, just before the minimum at $z$=1 $d_{peb}$, but exactly 0.5 $d_{peb}$ before the second maximum. Here the second layer of pebbles starts to contribute to the PF, resulting in a lower decrease of the PF. This pattern keeps repeating itself further away from the wall, damping out as the layers become less ordered due to the stochastic nature of the bed.

# 5 Measuring and Generating the 3D Pebble Bed Data

As mentioned in the introduction, after evaluating our computer generated beds using macroscopic stacking properties, we will look at the microscopic stacking properties on a pebble-to-pebble scale. For comparison, the locations of all pebbles in a pebble bed were experimentally determined using computer aided X-ray tomography, see Section 5.1. In Section 6 various microscopic stacking properties are compared with those of a computed bed, generated using the expanding system method described in Section 3, and with literature.

## 5.1 Measuring the 3D Pebble Bed Data

Computer aided X-ray tomography was used by Van Dijk [21] to create an image of a randomly packed pebble bed 42 mm high and with a diameter of 40.0 mm, containing 8920 pebbles. The pebbles were made of glass and had an average diameter of 1.93 mm, resulting in a $D_{bed}/d_{peb}$ ratio of 20.7. The average particle diameter of 1.93 mm was determined with an accuracy of 0.01 mm by first determining the average particle volume by measuring the volume of all particles and dividing it by the number of particles, and from that calculating the average particle diameter assuming perfectly spherical particles. Unfortunately the pebbles were neither perfectly spherical, nor very uniform in diameter. The distribution of the particle sizes is not known, as it was difficult to determine due to the particles not being perfectly spherical. Variations between the minimum and maximum diameter of a single particle depending on its orientation could easily vary 0.1 mm or more, with diameters for all particles ranging from 1.66 to 2.00 mm. To scan the bed it was encased in a cylinder made of PVC, and the top and bottom of the bed were constrained by steel wire-meshes, tightly fitted over the particles. Because of this tight fit, the top and bottom of the bed are slightly convex. Care was taken not to disturb the stacking while immobilising the bed with the steel wire-meshes, so that the pebble bed would remain uncompressed, albeit secured. See Figure 7 for an image of the bed reconstructed from the measured data.

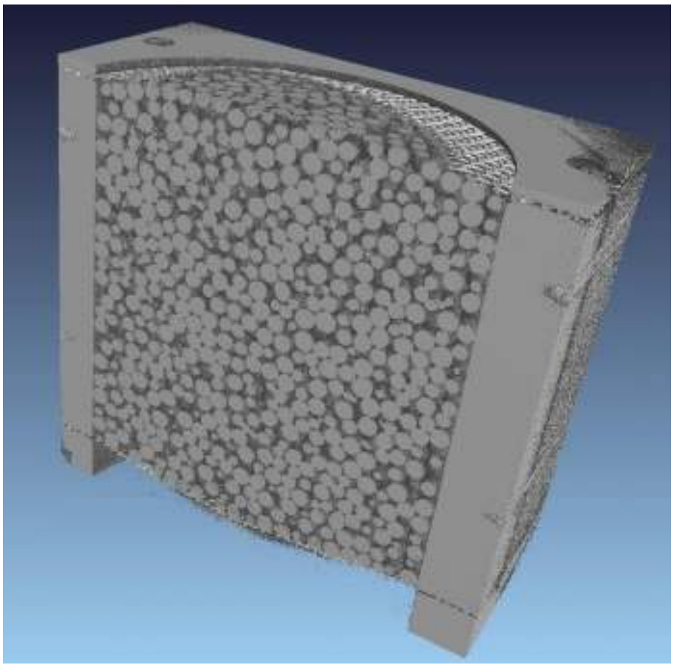

Figure 7: Image of the scanned bed with diameter 40 mm inside the placeholder, reconstructed using the voxels data [21].

The spatial resolution of the scan was 100 µm, about 20 times smaller than the pebble diameter. The output of the CT scanner is a greyvalue for each cell in the measuring domain, a 3D grid representing the spatial location of each cell. Each of these cells represents a volume pixel (voxel) of 100 by 100 by 100 µm. The greyvalue is a measure for the attenuation of the X-ray at the voxel location, and thus of the amount of solid material at the voxel. To translate the greyvalues to pebble-air data, a threshold value was chosen to translate them to either 0 (void) or 1 (pebble). In the rest of this paper we will refer to this data as the voxels data. To analyse the characteristics of the bed the positions of the centres of each sphere was needed. First, the amount of solid within a sphere of radius $R_{peb}$=0.965 mm was calculated at every voxel location. Next, this data was searched for maxima to obtain the pebble centre locations, which from now on we will refer to as the pebbles data. It should be noted that for constructing the pebbles data we assumed that all pebbles have the same radius $R_{peb}$=0.965 mm.

Various factors contribute to the uncertainty in the pebble locations of the resulting pebbles data set constructed from the X-ray scan. First, although the spatial resolution of the X-ray scanner was reported to be 10 µm [21], the actual voxel size in the experiment was 100 µm, resulting in a spatial uncertainty of 0.1 mm. Second, the resulting data from the scan was a grayvalue, which has an intrinsic uncertainty due to the stochastic process of X-ray scanning, and also includes uncertainties due to the algorithm used to construct the data for each voxel in the software of the scanning machine. From the greyvalue distribution reported by van Dijk [21] we can assume this effect is small for most voxels as the solid and void peaks in greyvalue lie far apart. However, near solid/void interfaces it is harder to determine whether a voxel is solid or void, and especially around interfaces of contacting pebbles this can result in a much larger solid area around the contact area of the two pebbles. This is even more problematic near the wall of the vessel, as there the contact between the convex pebble and the concave wall results in a relatively large space where the void gap is very small. We estimate that this effect adds another 0.1 mm uncertainty to the algorithm that finds the pebble centre locations, and possible more just next to the wall. Finally, we estimate the pebble size and shape distribution results in an uncertainty of up to 0.3 mm in determining the pebble centre locations, depending on the magnitude of the deviation in size and shape of the pebble under consideration from the average. Together this results in an estimated 0.1-0.3 mm uncertainty in the pebble locations. Additionally, there is also an uncertainty in where exactly the centre of the bed lies, and thus where the wall is, resulting in an uncertainty in the radial distance of a pebble from the wall, estimated to be 0.1 mm.

## 5.2 Computer Generated Bed

The computed bed was generated using the removing overlaps method detailed in Section 3. In the previous section, we showed that the computer generated beds accurately capture the macroscopic behaviour of real pebble beds. To investigate the microscopic properties a large bed was generated to ensure sufficient empirical data to construct accurate probability density functions of the various properties of the packing microstructure. The bed is cylindrical with a bed over pebble diameter factor of $D_{bed}/d_{peb}$=50, has a flat bottom, and contains 67500 pebbles. When analysing the bed, only the section between 5 and 25 pebble diameters from the bottom is used to make sure there are no effects from the bottom or top of the bed inside the domain under consideration.

## 5.3 Radial and Average Packing Fraction

To investigate differences in packing structures in the bulk of the bed and near the wall, we investigated the properties of the beds in two separate regions, an inner and an outer zone. The inner zone is the part of the bed more than 2.5 $d_{peb}$ away from the wall, and the outer zone the part within 2.5 $d_{peb}$ from the wall, where fluctuations in the porosity profiles and thus wall effects are large. Although between 2.5 and 5 $d_{peb}$ from the wall fluctuations exists, these are strongly dampened, and stacking properties are expected to be similar to those in the centre of the bed. Also, the stacking properties analysed do not consider just a single pebble location, but also at the pebbles surrounding it, sometimes up to several pebble diameters away. Thus we decided to look for the inner zone at pebbles more than 2.5 $d_{peb}$ from the wall, to get a clear picture of stacking properties close to the wall, where wall effects on the packing are strong. When choosing a boundary between outer and inner zone further away from the wall, stacking properties for the two zones became similar, making it harder to distinguish between properties close to the wall and in the bulk of the bed. For both zones, we only consider the part of the bed at least 5 pebble diameters away from the top and bottom of the bed. The packing fractions of the inner and outer zones of the computed bed and the spheres and voxels data sets of the measured bed are given in Table 2 together with their total packing fraction. The radial packing fraction profile of the three data sets was also calculated, see Figure 8. The computed bed has a $D_{bed}/d_{peb}$ ratio of 50, so only the first part of its packing fraction profile is shown to better fit the figure. We have seen in Section 4 that the computational method generates beds with realistic average packing fractions and packing fraction profiles, so this comparison can tell us something of the quality of our measured spheres and voxels data sets.

Table 2: Packing fraction for inner (>2.5 $d_{peb}$ from wall), outer (<2.5 $d_{peb}$ from wall), and total volume for the three data sets.

| | Inner PF | Outer PF | Total PF |
|---|---|---|---|
| Computed | 0.634 | 0.624 | 0.632 |
| Scan - spheres | 0.633 | 0.608 | 0.622 |
| Scan - voxels | 0.646 | 0.620 | 0.635 |

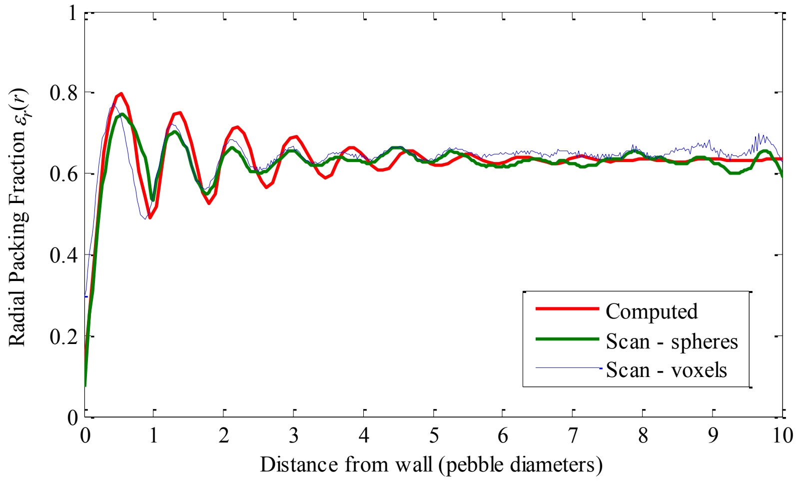


Figure 8: Radial packing fraction profile for the computed bed, for the voxels measurement data from the tomography scan, and for the pebble centre locations (spheres) derived from the voxels data.

First we see a significantly higher inner zone PF for the voxels data set than for the computed bed in Table 2 and in Figure 8 where the radial packing fraction for the voxels data is higher than the other two for $r$>5 $d_{peb}$. A possible cause could be the non-uniform pebble size and not perfectly spherical pebbles, resulting in a higher packing fraction, but it could also be a result of noise in the measurement data causing erroneous solid voxels in the void space between pebbles. The packing fraction of the outer zone of the voxels data and computed bed compare reasonably well, but that of the spheres data is lower. This is also visible in the radial packing fraction profile in Figure 8, where the spheres packing fraction is slightly lower than that of the voxels data. More importantly, there is also a mismatch between the spheres data and the voxels set in the shape of the profile <1 $d_{peb}$ to the wall. This suggests that near the wall our algorithm has trouble finding the correct location of the pebble centres from the voxels data, and for some pebbles it either cannot find the correct location or does not find the pebble at all, causing the lower packing fraction. A possible reason is the interference of the wall with the algorithm, where the solid voxels of the wall make it difficult to find the correct locations of the spheres. As was explained before, the large number of solid voxels making up the wall and surrounding the interfaces between the wall and pebbles in contact with it makes it harder for the algorithm to correctly identify the border between the pebble and the wall, resulting in a higher uncertainty as to the determined pebble centre locations in this region.

At a distance >1 $d_{peb}$ away from the wall the match between the three profiles is better. The scanned profiles are more dampened than the computed profile, but that is expected due to variations in pebble size, uncertainties in pebble locations, and measurement errors. The larger variations in packing fraction for the voxels and spheres data near the centre of the bed at $r$=10 $d_{peb}$ are also expected, as here the volume over which the profile is calculated becomes very small, causing statistical variations. In all three profiles the variations in packing fraction dampen out around 5 $d_{peb}$ from the wall as expected [1], and all three profiles show the same distance between the maxima and minima of the packing fraction profile. Summing up, the results give us a fair amount of confidence in the correctness of the spheres data set for most of the domain. Close to the wall more doubt on the accuracy of the spheres data set exists.

# 6 Pebble Bed Microscopic Stacking Properties

In this section various properties of the stacking microstructure of the computer generated and measured pebble beds are calculated and compared. From this point onward, when we talk about the scanned bed, we talk about the spheres data set of the measured bed, see Section 5.1, as the pebble centres are needed to determine the various stacking properties. As mentioned in Section 5.3, we have calculated the stacking properties of the outer zone near the wall and the inner zone separately to investigate possible spatial differences in the stacking properties.

## 6.1 Coordination Number

The coordination number of a sphere in a packing is the number of surrounding spheres in contact with that given sphere, and is a commonly investigated parameter in the literature on packed beds [13]. Besides being an important property of the local packing structure, it is also an important parameter for the effective thermal conductivity of a packed bed, as the pebble-to-pebble contact conduction is an important part of this [19, 22]. One of the inherent problems of the coordination number is how to define spheres in contact, especially when dealing with experimental data containing uncertainty. Here we follow a common approach to count all pebble centres within a certain distance $d_{peb}+\Delta$ of the reference pebble. In our case we use $\Delta=0.05\ d_{peb}$ so that we get the number of pebbles within 1.05 $d_{peb}$, identical to the approach followed by Aste [14]. The resulting probability density distribution of the coordination number for the inner and outer zones of the computed and scanned beds are depicted in Figure 9.

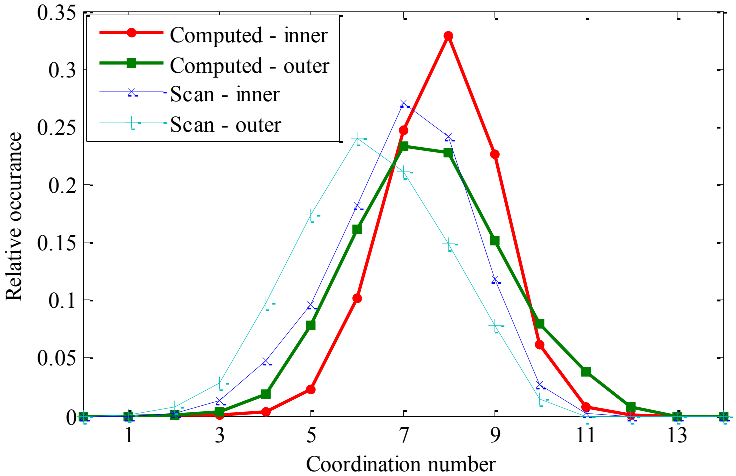


Figure 9: Distribution of the coordination number for the inner (bulk) and outer (near-wall) zones of the computed and measured bed. Pebbles within 1.05 $d_{peb}$ were counted as neighbours.

The theoretical maximum number of spheres touching a central sphere is 12, and indeed all four probability density functions of the coordination number have zero probability for 13 and up. To be stable, a pebble needs at least three contacts for support, which leads to a minimum value of the coordination number of three in the bulk of the bed, and two at the wall, where the wall can be one of the support contacts. Again, the probability density functions abide by this rule, although for the scanned bed in the outer zone there is a very small probability of one contact and in the inner zone of two contacts, which we contribute to uncertainties in the pebble locations and sizes.

The distributions of the coordination number of the inner zone of the computed bed shows a clear maximum at 8, with a probability around 0.33. Although the agreement with our scanned bed is not so good, agreement with the experimental results reported by Aste [14] is excellent, showing an almost identical shape of the distribution function. The lower coordination number of the scanned bed can be explained if we look at the radial distribution function discussed in Section 6.3, see Figure 11. Here the peak around 1 $d_{peb}$, relating to pebbles in (near) contact, shows a clear widening as a result of measurement and pebble size uncertainties, resulting in part of the peak falling outside the range $r<1.05\ d_{peb}$.

Comparing the results for the inner zones with those of the outer zones near the wall, both the scanned and the computed bed show peak values at a lower contact number for the outer zone, and in general a higher probability on lower contact numbers. This seems logical, as near the wall there is a lower packing fraction, see Table 2, and at the wall pebbles will have a lower contact number due to the wall itself. However, the computed bed shows in the outer zone also a higher probability for pebbles with a very high contact number of 10-12. These high contact numbers indicate a high level of ordering around some spheres, and correspond to the coordination number of hexagonal close packing.

## 6.2 Distribution of Packing Fraction of Voronoï Polyhedra

One way to look at the local distribution of space of spherical packings is by dividing the space into Voronoï polyhedral [23]. The Voronoï polyhedron around each pebble is formed by the space closest to the pebble centre with respect to any other pebble centre in the packing. To construct the polyhedra we used an algorithm detailed by Finney [24]. To calculate the Voronoï polyhedra for the pebbles close to the wall, imaginary pebbles were constructed such that the plane through the middle of their connection lines with the real pebble was tangent to the cylinder enclosing the pebble bed. Because several imaginary pebbles were used for each pebble, this method is fairly accurate, and will result in only a very small over-estimation of the volume of the Voronoï polyhedra at the wall.

The packing fraction of each individual Voronoï volume was calculated with $PF_i = V_{peb}/V_{Voronoï}$, and the results were used to construct the distribution of Voronoï packing fractions in Figure 10. Again the results were separated in an inner zone, with pebbles >2.5 $d_{peb}$ away from the wall, and an outer zone with pebbles within 2.5 $d_{peb}$ of the wall. Results are depicted for both the computed and the scanned bed, where the spheres data was used for the scanned bed. Due to the limited number of pebbles in the scanned bed, the data of the histograms contains significant stochastic variations. The same applies, although to a lesser degree, to the number of pebbles in the outer zone of the computed bed.

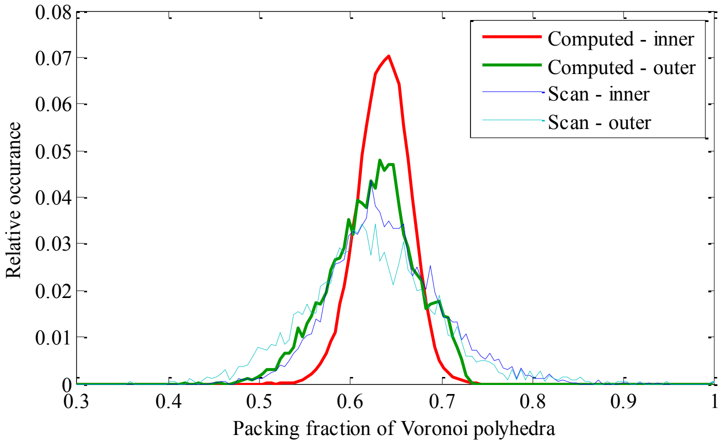


Figure 10: Distribution of the packing fraction of the Voronoï polyhedra for the inner (bulk) and outer zones (near-wall) of the computed and measured bed.

The distribution for the inner zone of the computed bed is non-symmetric with a longer tail at low PFs, a maximum occurring PF value of 0.736, and a minimum of 0.505, again similar to results found by Aste [14]. The outer zone of the computed bed has a lower peak value than the inner zone at the same PF, with a much broader and longer tail at low PF. This big tail at low PF, with a minimum PF of 0.415, is caused by the pebbles next to the wall. The maximum PF is the same as for the inner zone, corresponding to the maximum attainable packing fraction of 0.7405 for a hexagonal close packing. Finally we observe a higher probability of high PFs, suggesting a high ordering in the near-wall region of the stacking with pebbles forming closely packed layers parallel to the wall.

The packing fraction distributions for the scanned bed show a broader distribution than the computed distributions due to the variations in pebble size and uncertainties in measured pebble position. As we assume a uniform sphere diameter in the algorithm to find the sphere centres from the scan results, if the spheres in reality are smaller or larger, this will cause either gaps between spheres or overlapping spheres in the derived pebble centres data set. Also, errors in the derived sphere locations will result in sphere centres being either too far apart, resulting in gaps, or too close together, again resulting in overlapping spheres. This results in distorted polyhedra, where the packing fractions above 0.74 are caused by overlapping spheres. The significant number of polyhedra with these larger packing fractions indicate there are many overlapping pebbles in the spheres data set derived from the scan, and the fact some polyhedra have packing fractions of up to 1 for the inner zone show these overlaps can be large in this region. Still visible for the distribution of the outer zone is a lower peak and a larger probability of low packing fractions, but an increased probability of polyhedra with high packing fraction cannot be observed.

## 6.3 Radial Distribution Function

The radial distribution function $g(r)$ is often used in geometrical characterisation of packing structures to determine the correlation between particles within a system [13,14]. It is defined as the probability of finding the centre of a particle at distance $r$ from a reference one. We calculated $g(r)$ by counting the number of sphere centres $N$ in a shell with width $dr$=0.01 $d_{peb}$ around $r$ and using $g(r) = N / (V_{shell}/V_{peb})$ with $V_{shell}$ the volume of the shell around $dr$, so that for large $r$ $g(r)$ will tend to the average packing fraction. Results for the inner and outer zone of the computed and scanned bed are shown in Figure 11.

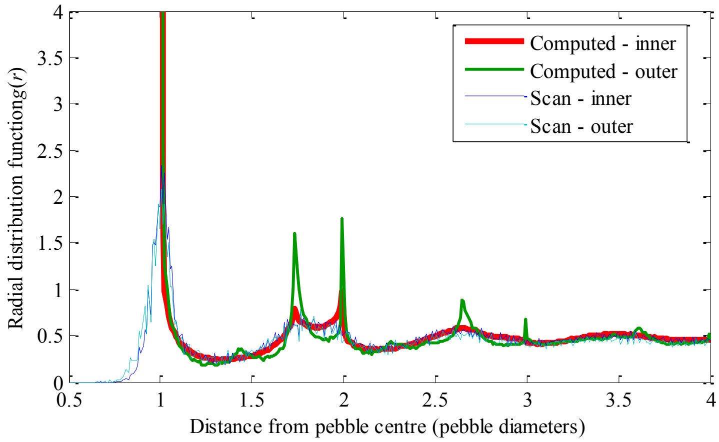


Figure 11: Radial distribution functions of the computed and scanned beds.

For the computed bed $g(r)$ has a sharp peak at 1 $d_{peb}$, associated with spheres in direct contact. Next there are two smaller peaks at $\sqrt{3}$ $d_{peb}$ and 2 $d_{peb}$, which were also observed in previous experiments [14] and simulations [13]. The peak at $\sqrt{3}$ $d_{peb}$ corresponds to four spheres forming a diamond of two equilateral triangles in the same plane, whereas the peak at 2 $d_{peb}$ is due to three spheres lying along a (rather) straight line. Although these smaller peaks indicate some ordering in the bed, the absence of further peaks for the inner zone and the small height of the peaks indicate this ordering is minor and on a very local scale only. In the outer zone however these peaks are much more pronounced, and $g(r)$ shows more peaks. These extra peaks correspond to typical distances in a hexagonal close packing, indicating that pebbles near the wall form planes parallel to the wall ordered in a roughly hexagonal pattern.

The results for the scanned bed show similar behaviour, although the peaks at $\sqrt{3}$ $d_{peb}$ and 2 $d_{peb}$ are much less resolved due to errors in position and variations in pebble size. For the outer zone no increase in ordering can be observed as there are no extra peaks. Question is if our computational bed is inaccurate in the near wall region, or if the absence of more peaks in the outer zone is due to errors in the measurement and data manipulation, or if the added randomness in the stacking due to variations in pebble size and sphericity result in less ordering in the scanned packing itself.

In light of this it is useful to look at $g(r)$ for $r$<1 $d_{peb}$, which gives a measure of the amount and size of overlaps in the spheres data reconstructed from the scan. Some overlap is acceptable, however, pebble centre distances as small as 0.65 $d_{peb}$ where observed, visible as non-zero values of $g(r)$ in Figure 11, indicating large overlaps exists in the spheres data. Also, the number of larger overlaps ($r$<0.9 $d_{peb}$) is significant, especially for the outer zone, with $g(r)$ values showing these large overlaps occur there more than twice as often as in the inner zone.

## 6.4 Distribution of Angles Between Spheres Touching a Common Neighbour

Another way to look at the level of ordering in the system is by looking at the angle between the contact lines of two pebbles with their common neighbour [13]. For the purpose of calculating these angles, we defined neighbours as being within 1.1 $d_{peb}$ of each other to account for uncertainties in pebble locations and size. For every pebble the angles of the contact lines with every pair of neighbours was calculated, resulting in the probability distributions in Figure 12. Again the results were split up into an outer zone with pebbles <2.5 $d_{peb}$ from the wall and an inner zone with pebbles further away.

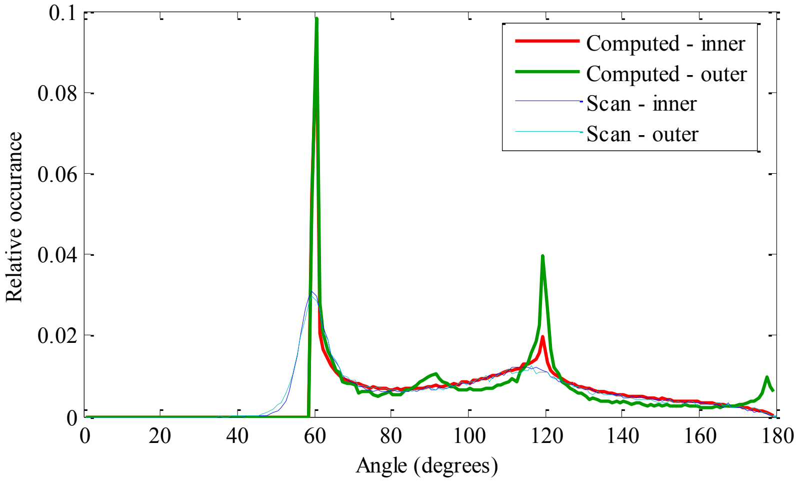


Figure 12: Distribution of the angles between the contact lines of two pebbles and their common neighbour.

All four distributions show a large peak at 60 degrees representing three pebbles touching each other, with the scanned beds showing a wider peak due to uncertainties. As with the radial distribution function, a significant amount of angles <60 degrees are observed for the scanned results, indicating overlaps, with the outer zone showing a larger number of smaller angles (<55 degrees) than in the inner zone. The four distributions also show a smaller peak at 120 degrees corresponding to four pebbles lying in the same plane forming a diamond, in line with the peak in the radial distribution function at √3 $d_{peb}$ in Figure 11. Again this peak is much wider and flatter for the scanned results. As before, there is hardly any difference between the inner and outer zone for the scanned bed, and they correspond well to the inner zone of the computed bed. However, the distribution of angles for the outer zone of the computed bed has significantly higher and sharper peaks, and also shows extra peaks at 90 and 180 degrees. These peaks correspond to a hexagonal closed packing, supporting our previous observations that near the wall the pebbles form more ordered planes of pebbles.

# 7 Distribution of Local Packing Fractions

In the previous section we looked at the microstructure in a pebble bed, investigating pebble-to-pebble ordering. In this section we investigate the probability distribution of packing fractions of small clusters of pebbles, as spatial variations in packing fraction might influence coolant flow and power density, and can be of importance for hotspot analysis. One could calculate the local packing fraction in a pebble bed by choosing a point, drawing a sphere around that point and computing the packing fraction within this sphere. However, the calculated packing fraction will then greatly depend on how well the surface of the sphere would coincide with pebble material or void space, meaning that small shifts in the location of the central point or in the chosen size of the sphere can result in large differences in resulting packing fraction. As a result, in a pebble bed with an ordered stacking and a uniform packing fraction, this method would result in a non-uniform distribution of the local packing fraction. To avoid this, in our eyes, arbitrary effect on the calculated packing fraction, we used the Voronoï polyhedra from Section 6.2.

To calculate the local packing fraction around a point in space, all pebbles with their centres closer than 2 $d_{peb}$ were selected, and the volumes of their Voronoï polyhedra were summed, which represents the volume occupied by the cluster of pebbles around the central point. From this the packing fraction was calculated by dividing the volumes occupied by the pebbles by the total volume of the Voronoï polyhedra. The size of these clusters was chosen to be big enough to influence flow and heat transfer, and small enough to capture local changes in packing density, with clusters containing around 45 pebbles. Using this method the local packing fraction was calculated at >60 million points throughout the computed bed and at >20 million points for the scanned bed. The resulting probability density distributions of the calculated cluster packing fractions are shown in Figure 13, were the results are split in cluster with centres >2.5 $d_{peb}$ away from the wall (inner zone), and an outer zone for cluster centres < 2.5 $d_{peb}$ to the wall.

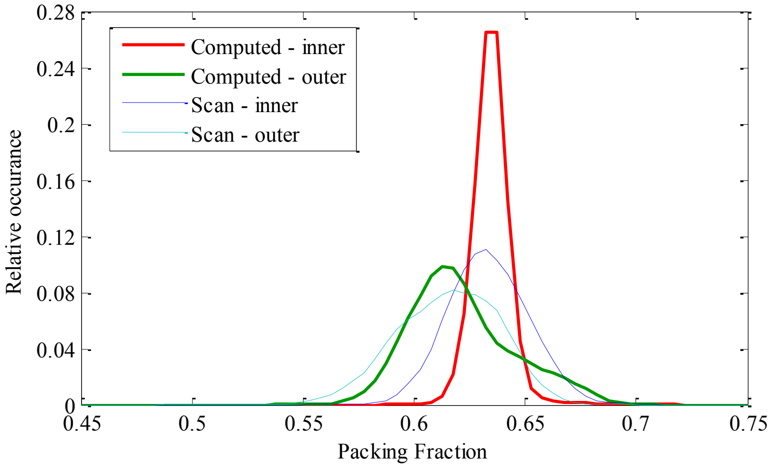


Figure 13: Probability density distribution of packing fractions of local pebble clusters in the inner and outer zones of the computed and scanned beds.

The distribution of packing fractions for the inner zone of the computed bed shows a very sharp peak around its average packing fraction of 0.634. However, not visible in the figure due to the low probability, is the occurrence of clusters with packing fractions of up to 0.7125, close to the maximum theoretical packing fraction of 0.740 for hexagonal close packing. The packing fractions for the inner zone of the scanned bed show a similar distribution, although broader due to the various uncertainties.

The outer zone of the computed bed, however, has a distinctly different distribution. The peak is much lower and at lower packing fraction, with lower packing fractions occurring due to the large void space around pebbles next to the wall. There is also a higher probability for areas with packing fractions above 0.65 than for the inner zone, which can be explained by an increased ordering close to the wall, resulting in an increase in areas with high local packing fraction, similar to the effect seen in Figure 10. The maximum packing fraction was slightly lower than for the inner zone, 0.7025, limited by the larger void space around pebbles next to the wall.

As before, agreement with results for the outer zone of the scanned bed is poor. Although that distribution also shows an increase of areas with lower packing fractions and a broader distribution, there is no increase but a decrease of areas with a high packing fraction. This could be caused by errors in the data acquisition and processing, or non-uniformity's in the pebbles causing more disorder in the near wall zone. Finally, there is the possibility that the larger curvature of the wall for the scanned bed, due to the smaller diameter, makes it harder for the pebbles to form ordered sheets parallel to the wall.

# 8 Conclusions

In pebble bed reactors the fuel pebbles form a randomly stacked bed through which the coolant flows. To investigate in detail flow, heat transfer and neutronics and find possible causes for hotspots, a good understanding of the nature of randomly stacked beds is necessary and tools to computationally generate realistic pebble beds are needed, whose macroscopic and microscopic pebble-to-pebble stacking properties are validated with experimental data.

To this end we accurately measured with the PebBEx facility the average packing fraction and radial and axial packing fraction profiles of randomly stacked beds containing 5400 acrylic pebbles with a uniform diameter of 12.7 mm. In a second experiment we used computer aided 3D X-ray tomography to determine the pebble locations of a randomly stacked bed of 8900 glass pebbles with diameters ranging from 1.66 to 2.00 mm, from which various properties of the packing microstructure were evaluated and local variations in packing fraction inside the bed were determined. Results from both experiments were compared with those of computed beds, generated using a numerical method we developed based on removing overlaps.

The macroscopic properties of the computed bed matched those of the PebBEx measurements very well, having an almost identical average packing fraction and radial and axial packing profiles similar to those of the experiment both in shape and in size of the fluctuations. The evaluated microscopic stacking properties from the 3D X-ray scan were the coordination number, distribution of Voronoï polyhedron packing fraction, radial distribution function, and the distribution of the angle between the contact lines of two spheres with a common neighbour. Properties were evaluated for both the bulk of the bed away from the wall, and the near wall region. For the bulk of the bed, there was a reasonably good match between the computed bed and experimental results from the 3D X-ray tomography, and an very good match with computational and experimental results from literature [13, 14]. In the near wall zone, the match was not so good. However, various properties of the experimentally determined pebble centre locations indicate the quality of the data is poor in the near wall region. First, the pebbles used for the scan were not very uniform in size. Also, significant overlap was observed between pebbles for the determined pebble centres, and the shape of the radial porosity profile near the wall matched poorly with accurate experimental results, both indications we were not successful in accurately determining the pebble locations near the wall. Taken together, the results show the computational method generates randomly stacked beds with realistic macroscopic and microscopic stacking properties. Although there is no gravity in the computational method and it cannot simulate pebble flow, the method creates beds without any overlaps with exactly touching pebbles, and is especially suitable to investigate in detail flow and heat transfer in small sections of a pebble bed. However, to be more confident of the microscopic stacking properties near the wall better experimental 3D stacking data is needed. Preferably by using a larger bed for more statistical data, but more importantly one with uniform pebble size, and an improved algorithm to better determine the pebble centre locations from the scan results, especially near the wall.

Results for both the radial and axial packing fraction profiles and the microscopic packing properties indicate the stacking structure of a randomly packed bed is different near the wall than in the bulk of the bed. Near the wall, the pebbles form semi-ordered layers with hexagonal-like stacking properties. As the layers lie parallel to the wall, the stacking near the wall is not isotropic. This indicates that to accurately describe flow and heat transfer, different models could be needed near the wall than in the bulk, and that flow and heat transfer might be anisotropic near a solid boundary.

Finally the experimental and computational results emphasise variations in the pebble stacking are inherent in randomly stacked beds. The location and size of peaks in the axial packing fraction profiles varied for two different beds, differences in filling procedures resulted in differences in average packing fraction, and the microscopic packing properties showed distributions of values over a wide range. The probability distributions of packing fractions of small clusters of around 45 pebbles showed strong variations in packing fractions exist inside a bed, both in the bulk and near the wall, which might significantly affect flow rates and could result in hotspots.

# 9 Annexe

Annex 1 – References

[1] R. F. Benenati and C. B. Brosilow. Void fraction distribution in beds of spheres. AIChE Journal, 8:359-361, 1962.

[2] J. Lieberoth and A. Stojadinović. Neutron streaming in pebble beds. Nuclear Science and Engineering, 76:336-344, 1980.

[3] G. J. Auwerda, J. L. Kloosterman, D. Lathouwers, and T. H. J. J. van der Hagen. Effects of random pebble distribution on the multiplication factor in HTR pebble bed reactors. Annals of Nuclear Energy, 37:1056-1066, 2010.

[4] G. J. Auwerda, Y. H. Zheng, D. Lathouwers, and J. L. Kloosterman. Effect of non-uniform porosity distribution on thermalhydraulics in a pebble bed reactor. In Proceedings of NURETH-14, Toronto, Ontario, Canada, September 25-29 2011.

[5] C. G. du Toit. Radial variation in porosity in annular packed beds. Nuclear Engineering and Design, 238:3073-3079, 2008.

[6] J. J. Cogliati and A. M. Ougouag. Pebbles: A computer code for modeling packing, flow and recirculation of pebbles in a pebble bed reactor. In Proceedings of HTR2006, 3rd International Topical Meeting on High Temperature Reactor Technology, Johannesburg, South-Africa, October 1-4 2006.

[7] C. H. Rycroft, G. S. Grest, J.W. Landry, and M. Z. Bazant. Analysis of granular flow in a pebble-bed nuclear reactor. Physical Review E, 74, 2006.

[8] J. L. Kloosterman and A. M. Ougouag. Comparison and extension of dancoff factors for pebble-bed reactors. Nuclear Science and Engineering, 157:16-29, 2007.

[9] W. van Antwerpen, P. G. Rousseau, and C. G. du Toit. Multi-sphere unit cell model to calculate the effective thermal conductivity in packed pebble beds of mono-sized spheres. Nuclear Engineering and Design, 247:183-201, 2012.

[10] D. Pavlidis and D. Lathouwers. Fluid flow and heat transfer investigation of pebble bed reactors using mesh-adaptive large-eddy simulation. In Proceedings of NURETH-14, Toronto, Ontario, Canada, September 25-29 2011.

[11] G. J. Auwerda, J. L. Kloosterman, D. Lathouwers, and T. H. J. J. van der Hagen. Packing microstructure and local density variations of experimental and computational pebble beds. In Proceedings of PHYSOR 2012, Knoxville, Tennessee, USA, April 15-20 2012.

[12] P. Mrafko. Homogeneous and isotropic hard sphere model of amorphous metals. Journal de Physique Colloques, 41(C8):322-325, 1980.

[13] W. S. Jodrey and E. M. Torey. Computer simulation of isotropic, homogeneous, dense random packing of equal spheres. Powder Technology, 30:111-118, 1981.

[14] T. Aste. Variations around disordered close packing. Journal of Physics: Condensed Matter, 17:S2361-S2390, 2005.

[15] V. J. J. van Dijk. Radial void fraction measurements of the pebble-bed inside a pebble-bed reactor. BSc. thesis, available through http://www.nera.rst.tudelft.nl/en/publications/, Delft University of Technology, Delft, 2008.

[16] J. Groen. Radial void fraction measurement of a random multisized pebble stacking. BSc. thesis, available through http://www.nera.rst.tudelft.nl/en/publications/, Delft University of Technology, Delft, 2009.

[17] Zongxin Wu, Dengcai Lin, and Daxin Zhong. The design features of the htr-10. Nuclear Engineering and Design, 218:25-32, 2002.

[18] G. D. Scott and D. M. Kilgour. The density of random close packings of spheres. Journal of Physics D: Applied Physics, 2:863-866, 1969.

[19] P. Baronner. Axiale void fractie van een willekeurig gestapeld pebble bed. Internship report, Delft University of Technology, Delft, 2012.

[20] G. E. Mueller. Radial void fraction distributions in randomly packed fixed beds of uniformly sized spheres in cylindrical containers. Powder Technology, 72:269-275, 1992.

[21] V. J. J. van Dijk. An efficient immersed boundary method based on penalized direct forcing for simulating flows through arbitrary porous media. Master's thesis, Delft University of Technology, Delft, 2011.

[22] W. van Antwerpen, P. G. Rousseau, and C. G. du Toit. Accounting for porous structure in effective thermal conductivity calculations in a pebble bed reactor. In ICAPP 2009, Tokyo, Japan, May 10-14 2009.

[23] C. F. Voronoï. Nouvelles applications des parametres continus a la théorie de formes quadratiques. Journal für die Reine und Angewandte Mathematik, 134:198-287, 1908.

[24] J. L. Finney. A procedure for the construction of voronoï polyhedra. Journal of Computational Physics, 32:137-143, 1979.